

# Electrochemiluminescence Mechanisms Investigated with Smartphone-Based Sensor Data Modeling, Parameter Estimation and Sensitivity Analysis

Elmer Ccopa Rivera,<sup>[a]</sup> Rodney L. Summerscales,<sup>[b]</sup> Padma P. Tadi Uppala,<sup>[c]</sup> and Hyun J. Kwon<sup>\*[a]</sup>

The present study introduces a unified framework combining a mechanistic model with a genetic algorithm (GA) for the parameter estimation of electrochemiluminescence (ECL) kinetics of the Ru(bpy)<sub>3</sub><sup>2+</sup>/TPrA system occurring in a smartphone-based sensor. The framework allows a straightforward solution for simultaneous estimation of multiple parameters which can be, otherwise, time-consuming and lead to non-convergence. Model parameters are estimated by achieving a high correlation between the model prediction and the measured ECL intensity from the ECL sensor. The developed

model is used to perform a sensitivity analysis (SA), which provides quantitative effects of the model parameters on the concentrations of chemical species involved in the system. The results demonstrate that the GA-based parameter estimation and the SA approaches are effective in analyzing the kinetics of the ECL mechanism. Therefore, these approaches can be incorporated as analysis tools in the ECL kinetics study with practical application in the calibration of mechanistic models for any required sensing condition.

## 1. Introduction

Recently, the smartphone-based electrochemiluminescence (ECL) sensor have been presented as a fast, low-cost and accurate alternative to expensive traditional instrumentation (such as the photomultiplier tube-based detectors) for analytical detection.<sup>[1,2]</sup> Smartphones devices are equipped with increasingly powerful processors for storage and analysis of data and have powerful data transmission capability. The use of these devices combined with certain accessory attachment (e.g., signal detectors) and advanced processing algorithms is a growing platform for different studies and applications, which in recent years, have focused on the prevention and monitoring of health.<sup>[3,4]</sup> For instance, smartphone-based sensors have been used for simultaneously detection of glucose and uric acid,<sup>[5]</sup> and glucose and blood

ketone<sup>[6]</sup> for disease diagnostic and treatment. More recently, literature has highlighted the significant role that these sensors can play in the detection of analytes confirming a viral infection, and in the vaccine development processing during pandemics.<sup>[7]</sup>


The Ru(bpy)<sub>3</sub><sup>2+</sup>/TPrA (Tris (2,2'-bipyridine) ruthenium(II)/tripropylamine) system whose ECL mechanism have been well established<sup>[8]</sup> is one of the most widely studied luminophore/coreactant systems in the field of ECL sensors. Optimizing the ECL performance (closely related to enhancement of the signal intensity) of smartphone-based sensors can be achieved by developing systematic methodologies to optimize the kinetic performance of existing luminophores and coreactants and also to design new ones. Therefore, it is necessary to study the kinetics of the Ru(bpy)<sub>3</sub><sup>2+</sup>/TPrA system occurring in a smartphone-based sensor to improve their ECL performance.

The kinetics of the ECL mechanism is investigated experimentally and through modeling, or a combination thereof with the help of different electrochemical techniques such as voltammetry<sup>[9–11]</sup> or chronoamperometry.<sup>[1,12,13]</sup> In these techniques, a time-varying waveform potential is applied to the working electrode, and the current and ECL time-series data can be measured. The applied potential triggers a series of reactions involving the ground state and intermediate species in the system. For modeling study, it is necessary to define suitable mathematical representation of reaction rates along with their parameters. As ECL intensity is strongly dependent on the sensing conditions, any changes in these conditions can influence all the parameters. Thus, it is necessary to estimate a set of optimal parameters simultaneously for each sensing condition. For this, it is ideal to generate the experimental measurements of all the chemical species involved in ECL reaction. Nevertheless, concentrations are often not amenable to experimental corroboration with the exception of uncommon studies such as the work of Danis

[a] Dr. E. C. Rivera, Dr. H. J. Kwon  
Department of Engineering  
Andrews University  
8450 E Campus Circle Drive  
Berrien Springs, MI 49104 (USA)  
E-mail: hkwon@andrews.edu

[b] Dr. R. L. Summerscales  
Department of Computing  
Andrews University  
4185 E. Campus Circle Drive  
Berrien Springs, MI 49103 (USA)

[c] Dr. P. P. Tadi Uppala  
School of Population Health, Nutrition & Wellness  
Andrews University  
8475 University Boulevard  
Berrien Springs, MI 49104 (USA)

 © 2020 The Authors. Published by Wiley-VCH GmbH. This is an open access article under the terms of the Creative Commons Attribution Non-Commercial License, which permits use, distribution and reproduction in any medium, provided the original work is properly cited and is not used for commercial purposes.

et al.,<sup>[14]</sup> in which concentration of  $\text{Ru}(\text{bpy})_3^{2+}$  was monitored *in situ* via spectroelectrochemistry and then it was used for modeling purposes. Difficulty arises as ECL intensity is the only observable output variable in the system.

Numerical studies to explore the kinetics of the ECL mechanism typically use ordinary or partial differential equations that constitute mechanistic models. This modeling approach is suitable for the mathematical description of reaction rates leading to the ECL generation. Recent literature presents some mechanistic models for the ECL mechanism with relevance and practical use in analytical electrochemiluminescence.<sup>[10,14,15]</sup> However, in most modeling works the parameters were not adjusted to the conditions studied, and only in a few studies the parameter estimation is carried out using trial-and-error methods. There is certainly a need for more systematic approaches.

The parameter estimation procedure for mechanistic models simulating the kinetics of the ECL mechanism can be very difficult to solve. The parameters need to be estimated simultaneously to effectively explain their effect on the kinetics of the ECL mechanism. Other challenges are related to the computational load to run multiple simulations for the parameter estimation procedure and other related techniques such as sensitivity analysis (SA). The high computational load of the space-time mechanistic models from literature can lead to extremely slow convergence times,<sup>[16]</sup> or non-convergence during the parameter estimation procedure and SA.

An accurate estimation of the parameters for mechanistic models naturally leads to a nonlinear optimization problem (NLP) containing nonlinear equations and continuous variables. For the study of the kinetics of the ECL mechanism, the aim of the NLP solving by an optimization algorithm can be to search for the optimum parameters that produces the best fit between the transient profile of the ECL measurements and that of the predicted luminophore excited state.<sup>[17]</sup> The optimization algorithms are an essential part of the parameter estimation techniques and they have been successfully applied in other branches of analytical chemistry such as electrochemical kinetics. For instance, the quasi-newton (QN) algorithm, a gradient-based algorithm<sup>[18]</sup> and the genetic algorithm, a stochastic algorithm (derivative-free)<sup>[19,20]</sup> greatly improved the parameter estimation accuracy in electrochemical mechanistic models.

In addition to estimating the optimal values of the model parameters, determining the identifiable influence of the parameters on the model outputs (time-course concentrations of the species) is essential to enhance the understanding of the ECL mechanism of the  $\text{Ru}(\text{bpy})_3^{2+}/\text{TPrA}$  system. A parameter is identifiable if it has a unique observable influence on the model outputs. The problem of parameter identifiability can be addressed using sensitivity analysis (SA).<sup>[21]</sup> This type of analysis can provide relevant information on the sensitivity of the model outputs for a range of variation of the parameters. Recent literature shows that SA is being used as part of modeling tools in different fields of electrochemistry.<sup>[21–24]</sup> However, to the best of the authors' knowledge, just as the optimization algorithms, the formal sensitivity analysis applied to mechanistic models describing the ECL mechanism has not been reported in the literature. A common approach to sensitivity analysis of mechanistic model

parameters is the one-at-a-time (OAT) approach (mathematically it is expressed using partial derivatives), in which only one parameter is changed at a time keeping others fixed at their nominal values. OAT can be computationally efficient, but the parameters are varied around a single set of parameter values, which is not suitable for the simultaneous analysis of all the parameters governing the reaction rates of the ECL mechanism. An alternative to the OAT local sensitivity analysis approach is the global sensitivity analysis approach such as fractional factorial design (FFD).<sup>[25]</sup> In FFD the effects of parameters on the model outputs are assessed by varying the parameters simultaneously over a large range of values.

The objectives of this study are two-fold. First, the estimation of the optimal values of the parameters governing the reaction rates behind the ECL mechanism under a particular sensing condition are carried out. For this, a unified framework is used, which combines a mechanistic model with a genetic algorithm and utilizes experimental measurements from a low-cost smartphone-based ECL sensor. Secondly, through a sensitivity analysis (SA), a deep understanding of the ECL mechanism of the  $\text{Ru}(\text{bpy})_3^{2+}/\text{TPrA}$  system is obtained by examining the influence of the parameters on the model outputs (the transient profiles of the concentrations of all the species). The fractional factorial design is selected to perform the SA because it is a multivariate approach that can show global sensitivities of individual parameters. The proposed methodology shows the potential benefits of genetic algorithm-based parameter estimation and the SA in the kinetic study of the ECL mechanism occurring in a smartphone-based sensor.

## Experimental Section

### Sensor Apparatus and Chemicals

Measurements of sequences of ECL imaging were performed using a smartphone-based ECL sensor apparatus. The sensor design interfaces with a custom compact potentiostat (in a three-electrode set-up) and a smartphone with a custom-made app controlling the potentiostat parameters and the phone camera. Disposable screen-printed carbon electrodes (DropSens, DRP-110) were used. Details of the sensor apparatus, the operation of the compact potentiostat circuit, and chemicals used have been described elsewhere.<sup>[1,13]</sup>

### ECL Experimental Data Generation

This study used intensity data from measurements carried out with the smartphone-based ECL sensor for estimating the mechanistic model parameters. The ECL data were determined using the chronoamperometric technique where a square waveform potential was applied to the carbon working electrode with 50  $\mu\text{L}$  of  $\text{Ru}(\text{bpy})_3^{2+}/\text{TPrA}$  sample solution. The potential of 1.2 V vs.  $\text{Ag}/\text{Ag}^+$  produced ECL intensity from the triggering of the reactions of the chemical species in the  $\text{Ru}(\text{bpy})_3^{2+}/\text{TPrA}$  system. Details of the chronoamperometric technique are presented elsewhere.<sup>[1,13]</sup> ECL images were recorded for different concentrations of  $\text{Ru}(\text{bpy})_3^{2+}$  distributed in a range of 0.625 to 5.0  $\mu\text{M}$ . From this data, a key feature was identified; the decay kinetics of ECL intensity, which was used for estimating the model parameters following a simulation-optimization framework described in the next section.

## 2. Results and Discussion

### 2.1. Modeling and Parameter Estimation

#### 2.1.1. ECL Mechanism and Theoretical Aspects

This section provides the mathematical development of the charge-transfer reactions and homogeneous reactions considered in the mechanistic model and the ordinary differential equations (conservation equations) relating the concentrations of  $\text{Ru}(\text{bpy})_3^{2+}$ ,  $\text{Ru}(\text{bpy})_3^{3+}$ ,  $\text{Ru}(\text{bpy})_3^+$ ,  $\text{TPrA}$ ,  $\text{TPrA}^{*+}$ ,  $\text{TPrA}^*$  and  $\text{Ru}(\text{bpy})_3^{2+*}$  (in mM) involved in the reactions. The mechanistic model accounted for the transient-state of the involved species in a homogeneous diffusion layer of the electrolyte solution. Figure 1 shows a schematic representation of the ECL mechanism of the  $\text{Ru}(\text{bpy})_3^{2+}/\text{TPrA}$  system<sup>[8]</sup> taking place in the smartphone-based ECL sensor.

The electrochemiluminescence and its related mechanism are being extensively investigated due to its important application as a platform of light-emitting sensors and an analytical detection technique.<sup>[11,15,26,27]</sup> This study does not intend to deepen theoretical studies of the ECL mechanism of the  $\text{Ru}(\text{bpy})_3^{2+}/\text{TPrA}$  system, but rather to illustrate that the parameter estimation procedure of a complex system can be a straightforward task. Thus, this study used the reaction mechanisms originally proposed by Miao et al.,<sup>[8]</sup> which are described in Eqs. (1)–(6). These reactions have been used for simulation purposes in several theoretical studies.<sup>[10,15,28]</sup>

#### 2.1.1.1. Charge-Transfer Reactions

The charge-transfer reactions through an oxidizing potential were assumed to convert  $\text{Ru}(\text{bpy})_3^{2+}$  into  $\text{Ru}(\text{bpy})_3^{3+}$ , and the neutral form of  $\text{TPrA}$  to a strong oxidant, the cation radical  $\text{TPrA}^{*+}$ , as shown in Eqs. (1) and (2), respectively.<sup>[8,28]</sup>

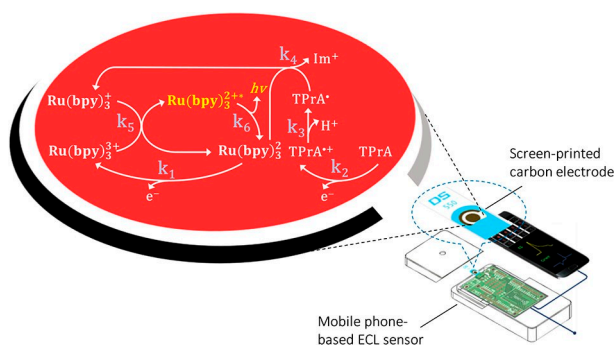


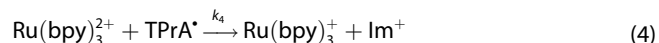
**Figure 1.** Schematic representation of the ECL mechanism taking place in the smartphone-based ECL sensor. The sensor apparatus is described in detail elsewhere.<sup>[11,13]</sup>

#### 2.1.1.2. Homogeneous Reactions

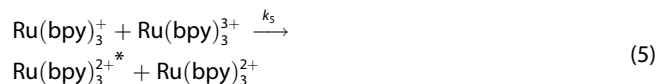
$\text{TPrA}^{*+}$  is assumed to be irreversibly deprotonated to form a free radical,  $\text{TPrA}^*$  as shown in Eq. (3).<sup>[8,15]</sup>



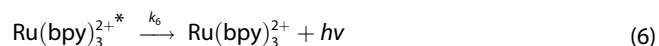
The electrogenerated radical  $\text{TPrA}^*$  undergoes an electron transfer oxidation with  $\text{Ru}(\text{bpy})_3^{2+}$ , thus reducing  $\text{Ru}(\text{bpy})_3^{2+}$  into  $\text{Ru}(\text{bpy})_3^+$ . At the electrode surface  $\text{TPrA}^*$  can also be oxidized into its corresponding iminium cation  $\text{Im}^+$ . This reaction is assumed to follow Eq. (4).<sup>[8,15,28]</sup>



The luminophore electronically excited state  $\text{Ru}(\text{bpy})_3^{2+*}$ , (Eq. (5)) is generated when  $\text{Ru}(\text{bpy})_3^{3+}$  formed by Eq. (1) reacts with  $\text{Ru}(\text{bpy})_3^+$  formed by the reaction between  $\text{Ru}(\text{bpy})_3^{2+}$  and  $\text{TPrA}^*$  (Eq. (4)).<sup>[8,10,15,28]</sup>



Then,  $\text{Ru}(\text{bpy})_3^{2+*}$  returns to the ground state specie  $\text{Ru}(\text{bpy})_3^{2+}$  by emitting a visible photon energy  $h\nu$ , as shown in Eq. (6).<sup>[8,10,15,28]</sup>



Current efforts at mechanistic modeling of the  $\text{Ru}(\text{bpy})_3^{2+}/\text{TPrA}$  system require simultaneous treatment of the reaction mechanisms shown in Eqs. (1)–(6).

#### 2.1.1.3. Conservation Equations

The conservation equations relating the concentrations of  $\text{Ru}(\text{bpy})_3^{2+}$ ,  $\text{Ru}(\text{bpy})_3^{3+}$ ,  $\text{Ru}(\text{bpy})_3^+$ ,  $\text{TPrA}$ ,  $\text{TPrA}^{*+}$ ,  $\text{TPrA}^*$  and  $\text{Ru}(\text{bpy})_3^{2+*}$  (in mM) involved in the charge-transfer and homogeneous reactions are presented by Eqs. (7)–(14).

$$\frac{d\text{Ru}(\text{bpy})_3^{2+}}{dt} = R_1 + R_5 + R_6 - R_4 \quad (7)$$

$$\frac{d\text{Ru}(\text{bpy})_3^{3+}}{dt} = -R_1 - R_5 \quad (8)$$

$$\frac{d\text{Ru}(\text{bpy})_3^+}{dt} = R_4 - R_5 \quad (9)$$

$$\frac{d\text{TPrA}}{dt} = R_2 \quad (10)$$

$$\frac{d\text{TPrA}^{*+}}{dt} = -R_2 - R_3 \quad (11)$$

$$\frac{d\text{TPrA}^*}{dt} = R_3 - R_4 \quad (12)$$

$$\frac{d\text{Ru}(\text{bpy})_3^{2+*}}{dt} = R_5 - R_6 \quad (13)$$

$$\frac{dh\nu_{\text{ECL}}}{dt} = R_6 \quad (14)$$

In Eqs. (7)–(14),  $R_1$  and  $R_2$  represent the charge-transfer reaction rates expressed by Eqs. (15) and (16), respectively, whereas  $R_3$  to  $R_6$  represent the homogeneous reaction rates expressed by Eqs. (17)–(20), respectively (mM/s).

$$R_1 = k_f^1 \times \text{Ru}(\text{bpy})_3^{3+} - k_b^1 \times \text{Ru}(\text{bpy})_3^{2+} \quad (15)$$

$$R_2 = k_f^2 \times \text{TPrA}^{*+} - k_b^2 \times \text{TPrA} \quad (16)$$

$$R_3 = k_3 \times \text{TPrA}^{*+} \quad (17)$$

$$R_4 = k_4 \times \text{Ru}(\text{bpy})_3^{2+} \times \text{TPrA}^* \quad (18)$$

$$R_5 = k_5 \times \text{Ru}(\text{bpy})_3^+ \times \text{Ru}(\text{bpy})_3^{3+} \quad (19)$$

$$R_6 = k_6 \times \text{Ru}(\text{bpy})_3^{2+*} \quad (20)$$

In this study, the parameters  $k_f^1$ ,  $k_b^1$ ,  $k_f^2$  and  $k_b^2$  in Eqs. (15) and (16) are modeled using the Butler-Volmer-type Eqs. (21) to (24), respectively.

$$k_f^1 = k_1 \times e^{(-\alpha \times f \times (E - E^0))} \quad (21)$$

$$k_b^1 = k_1 \times e^{((1-\alpha) \times f \times (E - E^0))} \quad (22)$$

$$k_f^2 = k_2 \times e^{(-\alpha \times f \times (E - E^0))} \quad (23)$$

$$k_b^2 = k_2 \times e^{((1-\alpha) \times f \times (E - E^0))} \quad (24)$$

where  $k_1$  and  $k_2$  ( $\text{s}^{-1}$ ) are the electron transfer rate parameters for the charge-transfer reactions shown in Eqs. (1) and (2), respectively,  $\alpha$  is the charge transfer coefficient taken as 0.5,  $f = F/RT$  ( $38.92 \text{ V}^{-1}$ ),  $E$  is the applied potential (1.2 V vs.  $\text{Ag}/\text{Ag}^+$ ), and  $E^0$  is the standard potential taken as 1.06 V vs.  $\text{Ag}/\text{Ag}^+$  for Eqs. (21) and (22) and 0.9 V vs.  $\text{Ag}/\text{Ag}^+$  for Eqs. (23) and (24). The mechanistic model simulating the ECL mechanism of the  $\text{Ru}(\text{bpy})_3^{2+}/\text{TPrA}$  system is formed using Eqs. (7)–(24). The model should allow the estimation of the parameters,  $k_1$  to  $k_6$  governing the reaction rates  $R_1$  to  $R_6$ .

### 2.1.2. Parameter Estimation Using Genetic Algorithm

A major issue in the development of a mechanistic model for the ECL mechanism is the accurate estimation of its parameters. In this study, the procedure to estimate the parameters ( $k_1$ – $k_6$ )

is formulated as a nonlinear optimization problem (NLP) as shown in Eq. 25.

$$\begin{aligned} \text{NLP : Min } & \psi(\theta) \\ \text{Subject to} & \\ \text{Eqs. (7 – 24), } & \theta_{\text{lb}} \leq \theta \leq \theta_{\text{ub}} \end{aligned} \quad (25)$$

where  $\psi$  is the objective function, and  $\theta_{\text{lb}}$  and  $\theta_{\text{ub}}$  are the lower- and upper-bound vectors, respectively for the parameter vector  $\theta$ . The aim of the parameter estimation procedure is to search for the optimum values of the parameters ( $\theta_{\text{optimum}}$ ) that produce the best fit between the transient profile of the measured ECL intensity (normalized to values of the order of magnitude of the predicted concentration of the excited state  $\text{Ru}(\text{bpy})_3^{2+*}$ ) and the corresponding computed transient profile of the concentration of  $\text{Ru}(\text{bpy})_3^{2+*}$  from the mechanistic model while minimizing  $\psi(\theta)$  given by Eq. (26). The normalization of the ECL intensity was based on previous observations by Danis et al.<sup>[17]</sup> that showed a close alignment between the transient profile of the measured ECL intensity and the predicted appearance of the transient profile of the luminophore excited state.

$$\psi(\theta) = \sum_{j=1}^{N_p} \frac{(y_{\text{exp}}(t_j) - y_{\text{sim}}(t_j))^2}{y_{\text{exp}(\text{max})}^2} \quad (26)$$

In Eq. (26),  $\theta$  is a vector containing all the parameters,  $y_{\text{exp}}(t_j)$  is the measured ECL intensity (normalized values) at sampling time  $j$ ,  $y_{\text{sim}}(t_j)$  is the concentration of the luminophore excited state computed by the mechanistic model,  $y_{\text{exp}(\text{max})}$  is the maximum measured ECL intensity, and  $N_p$  is the number of sampling points.

Since parameter estimation problem in Eq. (25) is nonlinear, nonconvex and has many unknown parameters, conventional gradient-based optimization methods can only guarantee convergence to a local solution. Also, the parameter estimation using conventional methods largely depends on the initial guesses of the parameter values, which can also lead to convergence issues. As an alternative to gradient-based optimization methods, this study investigated a derivative-free search approach based on genetic algorithm (GA) to solve Eq. (25). This approach, shown in Figure 2, combines a mechanistic model with a GA within a unified framework. A thorough exploration of the search space ( $\theta_{\text{lb}} \leq \theta \leq \theta_{\text{ub}}$ ) is performed by the GA toward the optimal solution, which consists in determining the optimum values for the parameters ( $\theta_{\text{optimum}}$ ). In this study, the GA based on the MyGA subroutine<sup>[29]</sup> was evaluated.

Figure 2 (in blue) shows the procedure used by the GA to estimate the parameters of the mechanistic model. First, a random population of individuals (chromosomes) was generated, which represents the parameters of the model within the search space. The search space is defined by the lower and upper limits on the parameters to be estimated. In this study, each chromosome is constituted by six genes, i.e., one numerical value for each parameter. The total number of chromosomes represents the population size in a generation. All generated individuals of the

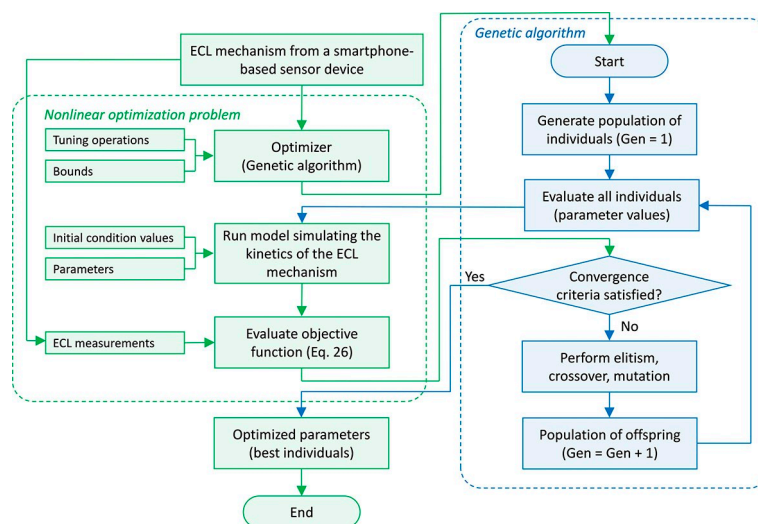


**Figure 2.** Framework that combines a mechanistic model with a genetic algorithm for the estimation of the parameters of the model simulating the kinetics of the ECL mechanism.

population representing different alternative models are simulated to estimate their fitness function defined by Eq. (26). This information is used to assign high scores for individuals with high fitness and low scores for individuals with low fitness. Individuals with low values for Eq. (26) are chosen for reproduction by crossover or mutation. Also, elitism is applied to copy the best individuals directly across to next generation. The reproduction consisting of the crossover and mutation operations is performed. The crossover operation exchanges genetic information (i.e., parameter values) from two parent individuals to generate two offspring individuals. Mutation changes one or more gene values in a parent individual to maintain genetic diversity. The crossover and mutation are carried out according to the crossover probability and mutation probability, respectively. The convergence criterion is the maximum number of generations. The optimal solution for the parameter estimation problem in the last generation reports the set of parameters ( $\theta_{\text{optimum}}$ ) that produce the lowest value of the fitness function, Eq. (26).

The nonlinear optimization problem (NLP) shown in Eq. (25) was implemented in a FORTRAN routine on an Intel(R) Core(TM) i7-7500 CPU @ 2.7 GHz. With these CPU characteristics, the time to solve the NLP was about three minutes for 2000 generations.

## 2.2. Sensitivity Analysis using Fractional Factorial Design

For sensitivity analysis (SA) purposes, the identifiable influence of the model parameters ( $k_1$ – $k_6$ ) on the model outputs, concentrations of  $\text{Ru}(\text{bpy})_3^{2+}$ ,  $\text{Ru}(\text{bpy})_3^{3+}$ ,  $\text{Ru}(\text{bpy})_3^+$ ,  $\text{TPrA}$ ,  $\text{TPrA}^+$ ,  $\text{TPrA}^\bullet$  and  $\text{Ru}(\text{bpy})_3^{2+*}$  were evaluated by using a  $2^{6-1}$  fractional factorial design (FFD).<sup>[30]</sup> In the FFD, the simulations involve systematically varying all parameters within  $\pm 20\%$  of optimal values calculated by the parameter estimation procedure. Statistical analysis of the data obtained in the FFD was performed using the software Statistica 10.0 (Statsoft Inc., USA).

The Pareto graph was used to evaluate the SA simulation results, which shows each of the estimated effects of the parameters on the model outputs. In this graph the size of each bar is relative to the standardized effect, calculated by dividing the estimated effect by its standard error, which represents a  $t$ -statistic. The size of the bars greater than the critical  $t$ -value was considered statically significant at the 95% significance level.

## 2.3. Kinetics Study Results of the ECL Mechanism

A series of chronoamperometric measurements were carried out using the smartphone-based ECL sensor. The ECL was measured at concentrations of  $\text{Ru}(\text{bpy})_3^{2+}$  of 5.0, 2.5, 1.25 and 0.625  $\mu\text{M}$  in an electrolyte solution with  $\text{TPrA}$  fixed at 20 mM. The concentrations of  $\text{Ru}(\text{bpy})_3^{2+}$  were in a range of practical use.<sup>[1,13]</sup>

To measure the ECL data for each concentration of  $\text{Ru}(\text{bpy})_3^{2+}$ , the sensor apparatus was set to apply a potential of 0 V vs.  $\text{Ag}/\text{Ag}^+$  for 1 s, followed by  $-1.2$  V vs.  $\text{Ag}/\text{Ag}^+$  for 1 s (stabilization period), and finally followed by 1.2 V vs.  $\text{Ag}/\text{Ag}^+$  for 1 s (oxidation period) as shown in Figure 3A. The ECL intensity recorded over the course of the stabilization and oxidation periods are shown in Figures 3B–E (red circles). These data clearly demonstrate that the ECL intensity exhibits a strong increase, reaches a peak, and then progressively decreases over time representing a decay kinetics. Understanding the kinetics of the ECL mechanism of this transient behavior is one of the main contributions of this study.

The genetic algorithm (GA) was used to estimate the model parameters ( $k_1$ – $k_6$ ). GA is able to find optimal or near-optimal solutions for parameter estimation problems with a wide search range. However, the use of an extremely large search space for a high-dimensional estimation problem (several parameters being optimized simultaneously) weakens the effects of the GA operators (crossover and mutation), producing premature convergence towards a local optimum. In premature convergence the

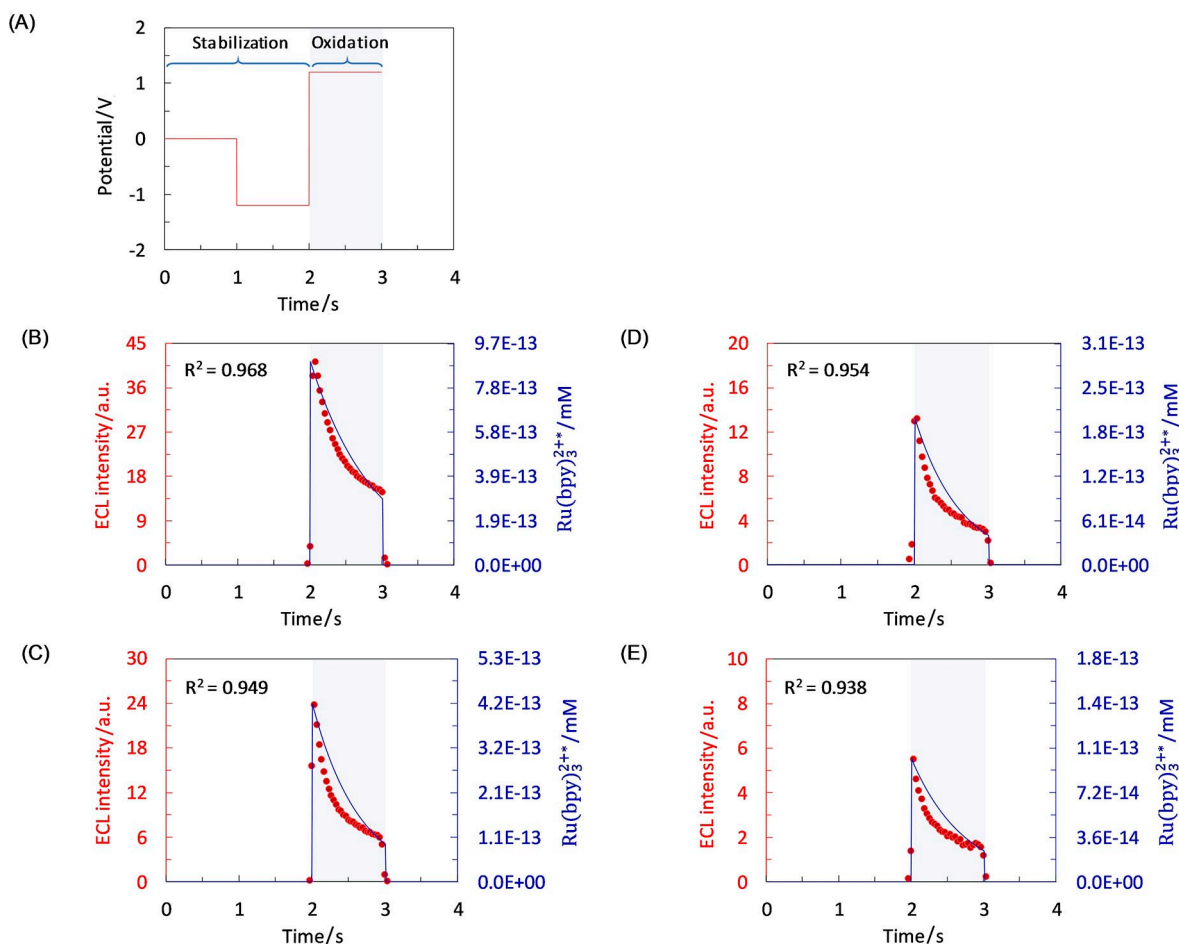


**Figure 3.** Electrochemiluminescence measurements and simulations: (A) Potential vs. time applied on carbon working electrode, and (B)–(E) comparison between the transient profile of the ECL experimental measurements (red circles) and the transient profile of the luminophore excited state  $\text{Ru}(\text{bpy})_3^{2+}$  predicted by the model (blue lines) at initial concentrations of  $\text{Ru}(\text{bpy})_3^{2+}$  of 5.0, 2.5, 1.25 and 0.625  $\mu\text{M}$ , respectively.

GA loses the diversity of the population of individuals during the optimization process. As a way to alleviate this problem, the present study used information from previous theoretical studies<sup>[10,11,15,16]</sup> to define the search range, which assisted the GA to perform well in terms of the rate of convergence. The literature does not explicitly show search ranges that may be used by the GA. However, certain key features such as the order of magnitude of the parameter values used in previous studies were taken into account for the definition of a relatively wide search range as shown in Table 1. The other GA operators/parameters were defined as follows: the initial population of the GA was set to 10 individuals or chromosomes (each chromosome is made up of

six genes, that is, a numerical value for each parameter), the maximum number of generations was 2000, the crossover probability was 0.8 and the mutation probability was 0.03. With the search space and GA operators defined, the GA performed an exhaustive exploration to estimate the optimal values of the parameters ( $k_1$ – $k_6$ ) such that Eq. (26) was minimized. The result of the parameter estimation yielded the establishment of the reaction rates constituting the mechanistic model for the specific sensing conditions of this study. Table 1 also shows the optimal values of the parameters with initial concentration of  $\text{Ru}(\text{bpy})_3^{2+}$  of 5.0  $\mu\text{M}$ . These optimal values were slightly fine-tuned to

**Table 1.** Search ranges for the genetic algorithm-based parameter estimation procedure and optimal values calculated for the model parameters.

Parameter	Unit	Search range for optimization		Optimal value	Reaction
		Lower bound	Upper bound		
$k_1$	( $\text{s}^{-1}$ )	0	0.0012	0.00048295	Eq. (1)
$k_2$	( $\text{s}^{-1}$ )	0	0.036	0.0018325	Eq. (2)
$k_3$	( $\text{mM}^{-1}\text{s}^{-1}$ )	0	3222	1747.107	Eq. (3)
$k_4$	( $\text{mM}^{-1}\text{s}^{-1}$ )	0	$5.00 \times 10^5$	$2.941 \times 10^5$	Eq. (4)
$k_5$	( $\text{mM}^{-1}\text{s}^{-1}$ )	0	500.0	225.329	Eq. (5)
$k_6$	( $\text{s}^{-1}$ )	0	$9.509 \times 10^4$	$5.253 \times 10^4$	Eq. (6)

improve the prediction of the model for the experimental data with different initial concentrations of  $\text{Ru}(\text{bpy})_3^{2+}$ .

Figures 3B–E illustrate that the transient profile of the ECL experimental measurements matched well with the transient profile of the concentration of the excited state  $\text{Ru}(\text{bpy})_3^{2+*}$ . The corresponding assessment using the correlation coefficient,  $R^2$  established that the model predictions were particularly accurate. These results demonstrate that the mechanistic model (Eqs. (7)–(24)) can be used to predict the kinetic behavior of the observable ECL intensity. Further, the present study demonstrates that the unified framework that combines the mechanistic model with a genetic algorithm can be straightforward, and it can be applied to any required detection conditions. This approach is an alternative to the trial-and-error method based in literature values, frequently

used in ECL theoretical studies.<sup>[11,15,16]</sup> The values of the parameters of a mechanistic model can vary significantly according to sensing conditions. The particular conditions of this study required a re-estimation of parameters, which was carried out satisfactorily using the proposed framework.

The model with the optimal values of the parameters is used to simulate the transient profiles of the concentrations of  $\text{Ru}(\text{bpy})_3^{2+}$ ,  $\text{Ru}(\text{bpy})_3^{3+}$ ,  $\text{Ru}(\text{bpy})_3^+$ , TPrA, TPrA<sup>•+</sup>, TPrA<sup>•</sup> and  $\text{Ru}(\text{bpy})_3^{2+*}$  represented by the black lines in Figures 4A–G. The green shading shows the region covered by the concentration profiles generated from the simulations of the sensitivity analysis addressed in the next section.

For the simulations results shown in Figure 4, it was assumed that the system was submitted to a potential pulse of 0 V vs. Ag/

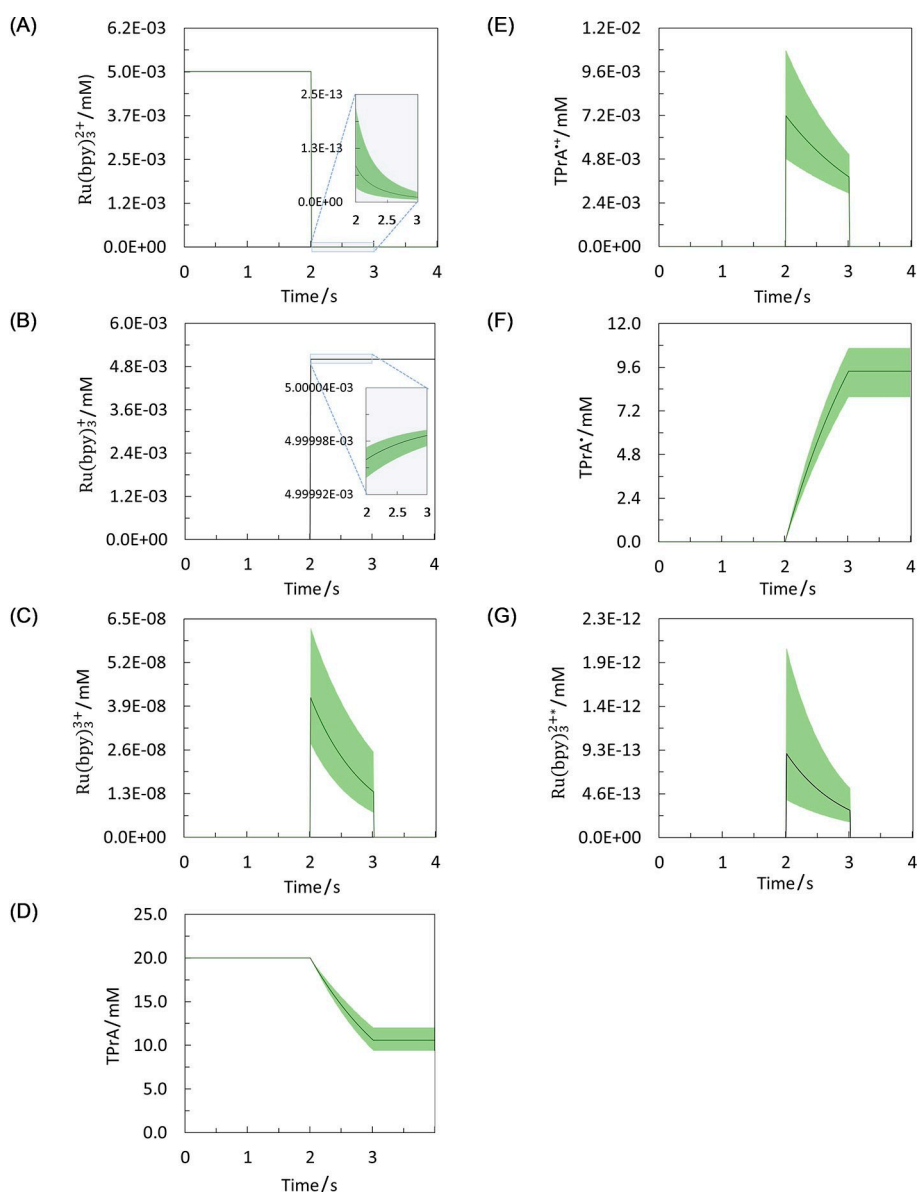


**Figure 4.** Simulations of the transient profiles of the concentrations of (A)  $\text{Ru}(\text{bpy})_3^{2+}$ , (B)  $\text{Ru}(\text{bpy})_3^+$ , (C)  $\text{Ru}(\text{bpy})_3^{3+}$ , (D) TPrA, (E) TPrA<sup>•+</sup>, (F) TPrA<sup>•</sup>, and (G)  $\text{Ru}(\text{bpy})_3^{2+*}$ . Black lines show the transient profiles of the concentrations calculated using the model with the optimal values from Table 1. The green shading shows the region covered by the thirty-two transient profiles of the concentrations of the species generated from the model simulations according to the fractional factorial design.

Ag<sup>+</sup> for 1 s, followed by  $-1.2$  V vs. Ag/Ag<sup>+</sup> for 1 s, and finally followed by  $1.2$  V vs. Ag/Ag<sup>+</sup> for 1 s (Figure 4A). Also, the modeling assumed a homogeneous diffusion layer of the electrolyte solution; thereby, the model derivatives were exclusively integrated with respect to time. Svir et al.<sup>[26]</sup> showed that simplified ECL models are computationally much faster than the detailed models (with time-space derivatives) for the optimization procedures. The same authors also demonstrated that a simplified model achieved similar performance to a detailed model when ECL transient profile was simulated. The strategy of integrating the model with respect to time adopted in this study allowed the simulations to show exclusively and explicitly the transient behavior of the concentrations of the species during the potential sweep as discussed below.

From Figures 4A–C and G it can be seen that the total concentration of the ruthenium species (i.e., an initial concentration  $[\text{Ru}(\text{bpy})_3^{2+}]_0$  of  $0.005$  mM) was mostly distributed between the  $\text{Ru}(\text{bpy})_3^{2+}$  and  $\text{Ru}(\text{bpy})_3^+$  species, which had extremely high reaction rates at early stage. The sum of the concentration of these species during the potential sweep was always nearby to  $[\text{Ru}(\text{bpy})_3^{2+}]_0$ , since  $\text{Ru}(\text{bpy})_3^{3+}$  and  $\text{Ru}(\text{bpy})_3^{2+*}$  (highly unstable intermediates) have extremely negligible concentrations as pointed out by Daviddi et al.<sup>[16]</sup> Indeed, the model predicted values of concentrations of  $\text{Ru}(\text{bpy})_3^{3+}$  and  $\text{Ru}(\text{bpy})_3^{2+*}$  of up to about  $6.5 \times 10^{-8}$  and  $2.0 \times 10^{-12}$  mM as shown in Figures 4C and 4G, respectively. Figure 4D shows a progressive decrease of the concentration profile of TPrA in its neutral form (from an initial concentration  $[\text{TPrA}]_0$  of  $20$  mM) during the potential sweep applied to the carbon electrode. This specie was irreversibly oxidized to generate the short-live cation radical  $\text{TPrA}^{\bullet+}$ .<sup>[26]</sup> The oxidation rate for TPrA neutral form shown in Figure 4 can vary significantly if electrodes with different materials are used as noted by Zu and Bard.<sup>[31]</sup> The  $\text{TPrA}^{\bullet+}$  specie deprotonates rapidly and irreversibly to form the strong reductant  $\text{TPrA}^\bullet$ , whose concentration profile calculated by the model is shown in Figure 4F. Figures 4D and F show that the sum of the concentration of TPrA neutral form and  $\text{TPrA}^\bullet$  throughout the potential sweep was always nearby to  $[\text{TPrA}]_0$ , since the  $\text{TPrA}^{\bullet+}$  intermediate specie rapidly deprotonated.<sup>[8]</sup> The model predicted  $\text{TPrA}^{\bullet+}$  concentrations of up to about  $1.0 \times 10^{-2}$  mM as shown in Figure 4E. The  $\text{TPrA}^\bullet$  specie undergoes a reaction with  $\text{Ru}(\text{bpy})_3^{2+}$  thereby reducing it to  $\text{Ru}(\text{bpy})_3^+$ , it reacts with  $\text{Ru}(\text{bpy})_3^{3+}$  to form the excited state luminophore,  $\text{Ru}(\text{bpy})_3^{2+*}$  (Figure 4G).<sup>[15]</sup> Finally,  $\text{Ru}(\text{bpy})_3^{2+*}$  deactivates through the emission of a visible photon energy.

The model with optimal values of the parameters from Table 1 is also used to perform a sensitivity analysis (SA) where the identifiable influence of the parameters  $k_1$ – $k_6$  on the model outputs were assessed.

## 2.4. Sensitivity Analysis Results

In this study the identifiable influence of the parameters ( $k_1$ – $k_6$ ) on the model outputs was determined using a  $2^{6-1}$  fractional factorial design (FFD). The parameters of the model were selected as factors and the model outputs were the transient profiles of the

concentrations of  $\text{Ru}(\text{bpy})_3^{2+}$ ,  $\text{Ru}(\text{bpy})_3^{3+}$ ,  $\text{Ru}(\text{bpy})_3^+$ , TPrA,  $\text{TPrA}^{\bullet+}$ ,  $\text{TPrA}^\bullet$  and  $\text{Ru}(\text{bpy})_3^{2+*}$ . Table 2 presents these factors and their corresponding values for each level. These values are  $\pm 20\%$  of the optimal values of the parameters in Table 1. Thirty-two-run were defined according to the  $2^{6-1}$  FFD. The results of the transient profiles of the model outputs for all runs are presented in Figures 4A–G, respectively. In these figures, the green shading shows the region covered by the thirty-two concentration profiles generated from the model simulations. From these data, a key feature was selected; the slope of the concentration profile, which was considered as the numerical response in the FFD.

The responses obtained from the statistical analysis of the FFD were evaluated by using Pareto graphs (Figures 5A–G). For ruthenium species ( $\text{Ru}(\text{bpy})_3^{2+}$ ,  $\text{Ru}(\text{bpy})_3^{3+}$ ,  $\text{Ru}(\text{bpy})_3^+$  and  $\text{Ru}(\text{bpy})_3^{2+*}$ ), the Figures 5A–C and G show that the effects of  $k_1$ ,  $k_2$ ,  $k_4$  and  $k_5$  are statically significant (at 95% significance level) on all these model outputs. The parameter  $k_3$  appeared significant only for  $\text{Ru}(\text{bpy})_3^+$ ,  $\text{Ru}(\text{bpy})_3^{3+}$  and  $\text{Ru}(\text{bpy})_3^{2+*}$ , whereas  $k_6$  is significant only for  $\text{Ru}(\text{bpy})_3^{2+*}$ . Figure 5 also shows that the significance ranking of the parameters was different for each model output. For instance, Figure 5G, in addition to showing that all parameters are significant on  $\text{Ru}(\text{bpy})_3^{2+*}$ , also shows that the parameter  $k_5$  governing reaction in Eq. (5) has an effect between three to six times greater on the referred model output than the parameters  $k_2$ – $k_4$ . The effects of parameters  $k_1$  and  $k_6$  have a similar order of magnitude and their effects are about 25% lower than the effect of  $k_5$ . These results show that the reaction between  $\text{Ru}(\text{bpy})_3^+$  and  $\text{Ru}(\text{bpy})_3^{3+}$  to form the excited state  $\text{Ru}(\text{bpy})_3^{2+*}$  (reaction in Eq. (5)) is the most critical reaction among those involving ruthenium species.

The study of the parameters influence on the transient profiles of the ruthenium species concentrations described above is important to understand the reactivity of this luminophore in the ECL mechanism of the  $\text{Ru}(\text{bpy})_3^{2+}/\text{TPrA}$  system.

The Pareto graphs in Figures 5D–F show that the effects of  $k_2$  are statistically significant for the transient profiles of all tripropylamine species in the system. The parameter  $k_3$  appeared significant only for  $\text{TPrA}^{\bullet+}$ . The crucial role that the cation radical  $\text{TPrA}^{\bullet+}$  plays in the  $\text{Ru}(\text{bpy})_3^{2+}/\text{TPrA}$  system is discussed below based on the simulation results of this study and from the literature.

The color matrix in Figure 6 can be used to display the parameter effects and combinations thereof on the model outputs at a glance. In this figure, all parameters were ranked by the brightness of the green color; the darker brightness

**Table 2.** Level of the parameters for sensitivity analysis using fractional factorial design.

Model Parameter	Level	
	–1	1
$k_1$	0.00038636	0.00057954
$k_2$	0.00146603	0.00219904
$k_3$	1397.685	2096.528
$k_4$	$2.35261 \times 10^5$	$3.52892 \times 10^5$
$k_5$	180.264	270.395
$k_6$	$4.20234 \times 10^4$	$6.30350 \times 10^4$



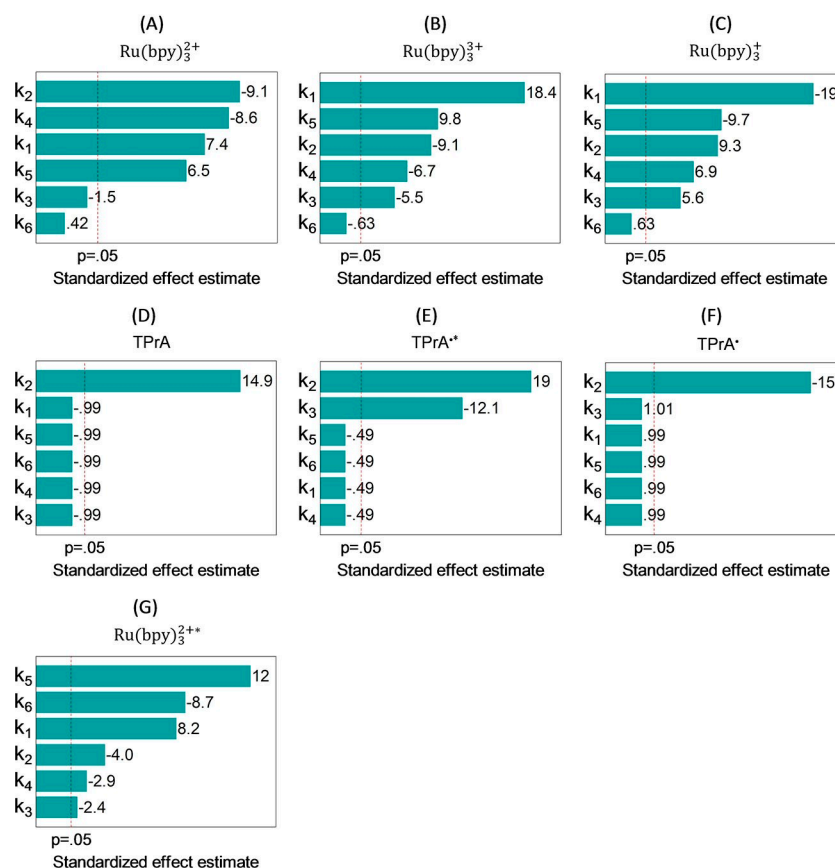


**Figure 5.** Pareto graphs of effects of the parameters on the model outputs: transient profiles of the concentrations of (A)  $\text{Ru}(\text{bpy})_3^{2+}$ , (B)  $\text{Ru}(\text{bpy})_3^+$ , (C)  $\text{Ru}(\text{bpy})_3^{3+}$ , (D) TPrA, (E) TPrA<sup>•+</sup>, (F) TPrA<sup>•</sup>, and (G)  $\text{Ru}(\text{bpy})_3^{2+*}$ .

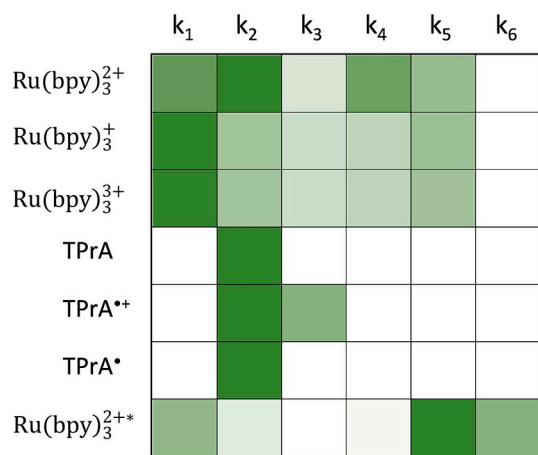


**Figure 6.** Parameter sensitivity ranking on the model outputs simulating the kinetics of the ECL mechanism.

means the higher ranking, that is, the most significant parameter. The results show that the parameter  $k_2$  that governs the oxidation reaction of TPrA to produce the cation radical TPrA<sup>•+</sup> (Eq. (2)) is significant, at different magnitudes, on the transient profiles of all species in the system, including the electrochemical generation of the excited state  $\text{Ru}(\text{bpy})_3^{2+*}$ . This finding implies the importance of the presence of TPrA<sup>•+</sup>

(and consequently the presence of the product of its deprotonation TPrA<sup>•</sup>) in the system for the electrochemical generation of  $\text{Ru}(\text{bpy})_3^{2+*}$ , which emits a visible photon energy, when it decays to the ground state  $\text{Ru}(\text{bpy})_3^{2+}$ . These results are supported by previous studies showing that the radicals TPrA<sup>•+</sup> and TPrA<sup>•</sup> are key species that should be present at the same time in the system for the electrochemical generation of the excited state  $\text{Ru}(\text{bpy})_3^{2+*}$ .<sup>[32]</sup> In other work,<sup>[33]</sup> 3D imaging approach showed that maximum ECL intensity occurs where concentrations of TPrA<sup>•+</sup> and TPrA<sup>•</sup> are locally the highest. On the other hand, a weaker ECL signal is consequence of the presence of oxygen-containing surface species which reduce the lifetime of TPrA<sup>•+</sup>, and therefore TPrA<sup>•</sup> would be susceptible to higher oxidative consumption subsequently (oxidation of TPrA<sup>•</sup> on the electrode). A recent work<sup>[34]</sup> focused on optimizing ECL signal performance, adopted a strategy to minimize oxygen and defects in the electrode surface with the goal of increasing the conductivity of the electrode and minimizing the oxidation of TPrA<sup>•</sup> on the electrode.

In this work, the sensitivity analysis, along with the genetic algorithm-based parameter estimation procedure, drive the systematic development of a reliable mathematical model for the ECL mechanism of the  $\text{Ru}(\text{bpy})_3^{2+}$ /TPrA system occurring in a smartphone-based sensor.

### 3. Conclusions

This article introduces a unified framework that combines a mechanistic model with a genetic algorithm to estimate the parameters governing the ECL mechanism of the Ru(bpy)<sub>3</sub><sup>2+</sup>/TPrA system. This approach overcomes the current limitations related to the complex nature and high computational load of the models. All ECL measurements, extracted from a low-cost smartphone-based ECL sensor, were in a close alignment with the simulated values. The results demonstrate that proposed framework is capable of establishing a well-adjusted mechanistic model, which simulates the kinetics of the ECL mechanism under specific sensing conditions. Further, the rapid convergence of the parameter estimation procedure (about three min for 2000 generations) can contribute to its practical application in the calibration of mechanistic models for any required sensing condition. The sensitivity analysis (SA) reveals the influence of the parameters on the model outputs and it demonstrates that the parameter  $k_2$  is particularly important in generating the excited state Ru(bpy)<sub>3</sub><sup>2+\*</sup>. In future work, the proposed approach can be used to explore the kinetics of the quenching mechanism of Ru(bpy)<sub>3</sub><sup>2+</sup>/TPrA electrochemiluminescence by economically relevant analytes such as phenolic compounds.

### Acknowledgements

The authors acknowledge National Science Foundation (grant number 1706597) for its financial support.

### Conflict of Interest

The authors declare no conflict of interest.

**Keywords:** sensors · smartphones · electrochemiluminescence · parameter estimation · sensitivity analysis

- [1] E. C. Rivera, J. J. Swerdlow, R. L. Summerscales, P. P. T. Uppala, R. Maciel Filho, M. R. Neto, H. J. J. S. Kwon, *Sensors* **2020**, *20*, 625.
- [2] X. Huang, D. Xu, J. Chen, J. Liu, Y. Li, J. Song, X. Ma, J. Guo, *Analyst* **2018**, *143*, 5339–5351.
- [3] W. Zhao, S. Tian, L. Huang, K. Liu, L. Dong, J. Guo, *Analyst* **2020**, *145*, 2873–2891.
- [4] A. Roda, E. Michelini, M. Zangheri, M. Di Fusco, D. Calabria, P. Simoni, *TrAC, Trends Anal. Chem.* **2016**, *79*, 317–325.
- [5] J. Guo, X. Ma, *Biosens. Bioelectron.* **2017**, *94*, 415–419.
- [6] J. Guo, X. Huang, X. Ma, *Sens. Actuators B* **2018**, *275*, 446–450.

- [7] N. Bhalla, Y. Pan, Z. Yang, A. F. Payam, *ACS Nano* **2020**, <https://dx.doi.org/10.1021/acsnano.0c04421>.
- [8] W. Miao, J.-P. Choi, A. J. J. Bard, *J. Am. Chem. Soc.* **2002**, *124*, 14478–14485.
- [9] J. Jin, F. Takahashi, T. Kaneko, T. J. E. Nakamura, *Electrochim. Acta* **2010**, *55*, 5532–5537.
- [10] K. Imai, G. Valenti, E. Villani, S. Rapino, E. Rampazzo, M. Marcaccio, L. Prodi, F. J. T. J. o P C C Paolucci, *J. Phys. Chem. C* **2015**, *119*, 26111–26118.
- [11] A. S. Danis, J. B. Gordon, K. P. Potts, L. I. Stephens, S. C. Perry, J. J. A. c Mauzeroll, *Anal. Chem.* **2019**, *91*, 2312–2318.
- [12] L. Dennany, C. F. Hogan, T. E. Keyes, R. J. J. A. c Forster, *Anal. Chem.* **2006**, *78*, 1412–1417.
- [13] H. J. Kwon, E. C. Rivera, M. R. Neto, D. Marsh, J. J. Swerdlow, R. L. Summerscales, P. P. T. J. R. i C Uppala, *Res. Chem.* **2020**, *2*, 100029.
- [14] A. S. Danis, K. P. Potts, S. C. Perry, J. J. A. c Mauzeroll, *Anal. Chem.* **2018**, *90*, 7377–7382.
- [15] M.-M. Chen, W. Zhao, M.-J. Zhu, X.-L. Li, C.-H. Xu, H.-Y. Chen, J.-J. J. C. s Xu, *Chem. Sci.* **2019**, *10*, 4141–4147.
- [16] E. Daviddi, A. Oleinick, I. Svir, G. Valenti, F. Paolucci, C. J. C. Amatore, *ChemElectroChem* **2017**, *4*, 1719–1730.
- [17] A. S. Danis, W. L. Odette, S. C. Perry, S. Canesi, H. F. Sleiman, J. J. C. Mauzeroll, *ChemElectroChem* **2017**, *4*, 1736–1743.
- [18] A. N. Simonov, G. P. Morris, E. Mashkina, B. Bethwaite, K. Gillow, R. E. Baker, D. J. Gavaghan, A. M. J. A. c Bond, *Anal. Chem.* **2016**, *88*, 4724–4732.
- [19] S. Zhou, L. Bu, Z. Shi, L. Deng, S. Zhu, N. J. J. o h m Gao, *J. Hazard. Mater.* **2018**, *346*, 73–81.
- [20] M. Weng, X. J. F. i c Yu, *Front Chem.* **2019**, *7*.
- [21] A. Goshtasbi, J. Chen, J. R. Waldecker, S. Hirano, T. J. J. o t E S Ersal, *J. Electrochem. Soc.* **2020**, *167*, 044504.
- [22] Q. Lai, S. Jangra, H. J. Ahn, G. Kim, W. T. Joe, X. Lin, *2019 American Control Conference (ACC)*, IEEE **2019**, pp. 890–896.
- [23] Q. Shao, E. Gao, T. Mara, H. Hu, T. Liu, A. J. A. E. Makradi, *Appl. Energy* **2020**, *260*, 114318.
- [24] K. Jiang, X. Liu, G. Lou, Z. Wen, L. J. J. o P S Liu, *J. Power Sources* **2020**, *451*, 227821.
- [25] A. Saltelli, T. Andres, T. J. C. s. Homma, D. Analysis, *Comput. Stat. Data An.* **1995**, *20*, 387–407.
- [26] I. Svir, A. Oleinick, O. Klymenko, C. Amatore, *Analytical Electrogenerated Chemiluminescence: From Fundamentals to Bioassays* (Ed.: N. Sojic), Royal Society of Chemistry, UK **2020**, pp. 134–155.
- [27] K. G. Cho, J. I. Lee, S. Lee, K. Hong, M. S. Kang, K. H. J. A. F. M. Lee, *Adv. Funct. Mater.* **2020**.
- [28] O. V. Klymenko, I. Svir, C. J. C. Amatore, *ChemPhysChem* **2013**, *14*, 2237–2250.
- [29] A. B. H. Yedder, *Numerical Optimization and Optimal Control: Applications in Molecular Chemistry*, Ph.D. diss. (in French), Ecole National des Ponts et Chaussées **2002**, pp. 227.
- [30] D. C. Montgomery, *Design and Analysis of Experiments*. John Wiley & Sons, Hoboken, NJ **2013**, pp. 752.
- [31] Y. Zu, A. J. J. A. c Bard, *Anal. Chem.* **2001**, *73*, 3960–3964.
- [32] Z. Chen, Y. J. T. J. o P C C Zu, *J. Phys. Chem. C* **2009**, *113*, 21877–21882.
- [33] M. Sentic, M. Milutinovic, F. Kanoufi, D. Manojlovic, S. Arbault, N. J. C. S. Sojic, *Chem. Sci.* **2014**, *5*, 2568–2572.
- [34] G. Valenti, M. Zangheri, S. E. Sansaloni, M. Mirasoli, A. Penicaud, A. Roda, F. J. C. A. E. J. Paolucci, *Chem. Eur. J.* **2015**, *21*, 12640–12645.

Manuscript received: June 4, 2020

Revised manuscript received: July 7, 2020